JPn Neuroscience
The Journal of Physiology
J Physiol 593.13 (2015) pp 2909–2926

State-dependent control of breathing by the retrotrapezoid nucleus

Peter G.R. Burke[1], Roy Kanbar[2], Tyler M. Basting[1], Walter M. Hodges[1], Kenneth E. Viar[1], Ruth L. Stornetta[1] and Patrice G. Guyenet[1]

[1] *Department of Pharmacology, University of Virginia, Charlottesville, VA 22908, USA*
[2] *Department of Pharmaceutical Sciences, Lebanese American University, Beyrouth, Lebanon*

Key points

- This study explores the state dependence of the hypercapnic ventilatory reflex (HCVR). We simulated an instantaneous increase or decrease of central chemoreceptor activity by activating or inhibiting the retrotrapezoid nucleus (RTN) by optogenetics in conscious rats.
- During quiet wake or non-REM sleep, hypercapnia increased both breathing frequency (f_R) and tidal volume (V_T) whereas, in REM sleep, hypercapnia increased V_T exclusively.
- Optogenetic inhibition of RTN reduced V_T in all sleep–wake states, but reduced fR only during quiet wake and non-REM sleep. RTN stimulation always increased V_T but raised f_R only in quiet wake and non-REM sleep.
- Phasic RTN stimulation produced active expiration and reduced early expiratory airflow (i.e. increased upper airway resistance) only during wake.
- We conclude that the HCVR is highly state-dependent. The HCVR is reduced during REM sleep because f_R is no longer under chemoreceptor control and thus could explain why central sleep apnoea is less frequent in REM sleep.

Abstract Breathing has different characteristics during quiet wake, non-REM or REM sleep, including variable dependence on P_{CO_2}. We investigated whether the retrotrapezoid nucleus (RTN), a proton-sensitive structure that mediates a large portion of the hypercapnic ventilatory reflex, regulates breathing differently during sleep *vs.* wake. Electroencephalogram, neck electromyogram, blood pressure, respiratory frequency (f_R) and tidal volume (V_T) were recorded in 28 conscious adult male Sprague–Dawley rats. Optogenetic stimulation of RTN with channelrhodopsin-2, or inhibition with archaerhodopsin, simulated an instantaneous increase or decrease of central chemoreceptor activity. Both opsins were delivered with PRSX8-promoter-containing lentiviral vectors. RTN and catecholaminergic neurons were transduced. During quiet wake or non-REM sleep, hypercapnia (3 or 6% F_{I,CO_2}) increased both f_R and V_T whereas, in REM sleep, hypercapnia increased V_T exclusively. RTN inhibition always reduced V_T but reduced f_R only during quiet wake and non-REM sleep. RTN stimulation always increased V_T but raised f_R only in quiet wake and non-REM sleep. Blood pressure was unaffected by either stimulation or inhibition. Except in REM sleep, phasic RTN stimulation entrained and shortened the breathing cycle by selectively shortening the post-inspiratory phase. Phasic stimulation also produced active expiration and reduced early expiratory airflow but only during wake. V_T is always regulated by RTN and CO_2 but f_R is regulated by CO_2 and RTN only when the brainstem pattern generator is in autorhythmic mode (anaesthesia, non-REM sleep, quiet wake).

DOI: 10.1113/JP270053

The reduced contribution of RTN to breathing during REM sleep could explain why certain central apnoeas are less frequent during this sleep stage.

(Resubmitted 11 December 2014; accepted after revision 19 March 2015; first published online 27 March 2015)
Corresponding author P.G. Guyenet, PhD: University of Virginia Health System, P.O. Box 800735, 1300 Jefferson Park Avenue, Charlottesville, VA 22908-0735, USA. E-mail: pgg@virginia.edu

Introduction

The retrotrapezoid nucleus (RTN) is a small cluster of lower brainstem neurons that are activated by hypercapnia and regulate several aspects of breathing, including inspiratory amplitude, breathing frequency and active expiration (Marina *et al.* 2010; Guyenet, 2014; Basting *et al.* 2015). The high responsiveness of RTN neurons to CO_2 *in vivo* is attributed to several mechanisms: an intrinsic sensitivity to protons, paracrine effects from surrounding pH/CO_2-sensitive astrocytes and inputs from other chemosensory neurons and the carotid bodies (Guyenet *et al.* 2005, 2010; Gestreau *et al.* 2010; Gourine *et al.* 2010; Huckstepp & Dale, 2011; Ramanantsoa *et al.* 2011; Wang *et al.* 2013). RTN neurons can therefore be viewed as central respiratory chemoreceptors (CRCs) that also function as chemoreflex integrator. These neurons mediate a large portion of the hypercapnic ventilatory reflex (HCVR) (Gestreau *et al.* 2010; Guyenet *et al.* 2010; Ramanantsoa *et al.* 2011; Wang *et al.* 2013).

The chemoreflex control of breathing is state-dependent. For example, although the respiratory chemoreflexes still operate during REM sleep, the breathing frequency (f_R) is typically unaffected by hypoxia or hypercapnia (Coote, 1982; Berthon-Jones & Sullivan, 1984; Horner *et al.* 2002; Lovering *et al.* 2003; Nakamura *et al.* 2007). In addition, in conscious cats ventilated to apnoea during non-REM sleep, diaphragmatic EMG re-emerges during REM sleep (Orem *et al.* 2005).

Periodic breathing occurs during sleep under hypobaric hypoxia, in patients with congestive heart failure, or after chronic opiate treatment (Berssenbrugge *et al.* 1983; Burgess, 1997; Farney *et al.* 2003; Weil, 2004). The apnoeas have been tentatively attributed to recurrent episodes of CNS hypocarbia that silence CRCs (Dempsey *et al.* 2012; Marcus *et al.* 2014). This interpretation agrees with the finding that respiratory alkalosis silences RTN in conscious rats (Basting *et al.* 2015). In adult humans or cats, periodic breathing occurs only during non-REM sleep (Berssenbrugge *et al.* 1983; Farney *et al.* 2003; Lovering *et al.* 2012).

Congenital central hypoventilation syndrome (CCHS) is caused by *Phox2b* mutations (Amiel *et al.* 2003; Weese-Mayer *et al.* 2010). This disease is characterized by the loss of breathing automaticity during sleep and a greatly reduced HCVR (Amiel *et al.* 2003; Weese-Mayer *et al.* 2010). In mice, *Phox2b* mutations abort RTN development, which probably causes most of the HCVR deficit (Ramanantsoa *et al.* 2011). In patients with CCHS, breathing is much better maintained during REM than non-REM sleep (Fleming *et al.* 1980). In short, reduced CRC activity resulting from carotid body hyperactivity (hypoxia, congestive heart failure) (Marcus *et al.* 2014) or RTN lesion (putative cause of CCHS) appears to cause central sleep apnoea selectively during non-REM sleep.

The purpose of this study was to examine the state dependence of the HCVR. We simulated an instantaneous increase or decrease of CRC activity by activating or inhibiting the RTN optogenetically (Abbott *et al.* 2009; Basting *et al.* 2015). We then measured the resulting effects on breathing during periods of quiet wake, non-REM or REM sleep.

Methods

Animals

Experiments were performed on male Sprague–Dawley rats ($n = 28$; 400–550 g; Taconic, Germantown, NY, USA). All procedures conformed to the NIH Guide for the Care and Use of Laboratory Animals and were approved by the University of Virginia Animal Care and Use Committee. Animals were housed under standard 12 h light/dark cycle with ad libitum access to food and water.

Lentiviral constructs and vector preparation

This study used lentiviral vectors (LVV) that express their transgene under the control of the Phox2b-responsive artificial promoter PRSx8 (Hwang *et al.* 2001). When injected into the rostral ventrolateral medulla or ventrolateral pons (noradrenergic 'A5' area) as described in this study, these LVVs transduce Phox2b-expressing neurons that are virtually exclusively catecholaminergic (C1 and A5 neurons) and RTN neurons (Abbott *et al.* 2009). One of the LVVs (PRSx8-ChR2-mCherry) encoded the photoactivatable cation channel channelrhodopsin-2 (ChR2, H134R) fused to mCherry (Abbott *et al.* 2009) and the other the photoactivatable proton pump archaerhodopsin (ArchT3.0) fused to eYFP (PRSx8-Arch-eYFP) (Han *et al.* 2011; Mattis *et al.* 2012; Basting *et al.* 2015). The vectors were produced by the University of North Carolina virus core and diluted to a final titre of 3.0×10^8 viral particles per ml with sterile phosphate-buffered saline. We verified that the above viral dilution transduced Phox2b-expressing neurons selectively (Fig. 9).

Injections of virus and instrumentation

We used two different approaches for targeting Arch or ChR2 to RTN neurons: Arch was delivered bilaterally to transduce RTN neurons *en masse* in both rostral and caudal regions and the optical fibres were targeted to the caudal RTN to illuminate the region with the highest density of RTN neurons (Takakura *et al.* 2008). By contrast, we restricted ChR2 expression to the rostral portion of the RTN on the left side. This was done to photoactivate RTN neurons without involving the C1 neurons whose photoactivation produces arousal and boost breathing via glutamatergic mechanisms (Abbott *et al.* 2013*b*, 2014; Burke *et al.* 2014).

For LVV injection, the rats were anaesthetized with a mixture of ketamine (75 mg kg^{-1}), xylazine (5 mg kg^{-1}) and acepromazine (1 mg kg^{-1}) given intraperitoneally (I.P.). The correct plane of anaesthesia was assessed by the absence of the corneal and hind-paw withdrawal reflexes. Additional anaesthetic was administered as necessary during surgery (25% of the original dose, I.P. or intramuscular). Body temperature was kept close to 37°C with a servo-controlled heating pad and a blanket. Rats received postoperative ampicillin (125 mg kg^{-1}, I.P.), and ketoprofen [3–5 mg kg^{-1}, subcutaneous (S.C.)] for two consecutive days. All surgical procedures were performed under aseptic conditions. The hair over the skull, neck and cheek were removed and skin disinfected. An incision over the mandible was made to expose the facial nerve for antidromic activation of facial motor neurons. The rat was then placed prone on a stereotaxic apparatus (bite bar set at −3.5 mm for flat skull; David Kopf Instruments Tujunga, CA, USA). A 1.5 mm diameter hole was drilled into the occipital plate on the left side (ChR2) or both sides (Arch) caudal to the parieto-occipital suture. Viral solutions were loaded into a 1.2 mm internal diameter glass pipette broken to a 25 μm tip (external diameter). To target the rostral RTN region with ChR2, the pipette was inserted at a 12–14 deg angle pointing towards the front of the animal and injections of 100–140 nl were made at two sites separated 200 μm (maximum 280 nl). These sites were located 100–200 μm below the rostral end of the facial motor nucleus whose lower edge was identified in each rat by mapping antidromic-evoked potentials elicited by stimulating the facial nerve (Brown & Guyenet, 1985). The Arch-LVV was injected bilaterally into four sites separated by 200 μm (total volume 400–600 nl side^{-1}), extending rostrally from the caudal end of the facial motor nucleus.

We then implanted electrodes for recording the electroencephalogram (EEG), neck electromyogram (EMG) and optical fibre–ferrule assemblies for light stimulation (Sparta *et al.* 2012). For EEG recordings, stainless steel jeweller screws (Plastics One, Roanoke, VA, USA) were implanted extradurally (0.5–1 mm anterior, 1 mm lateral to bregma and 3 mm posterior, 2–2.5 mm lateral to bregma above the contralateral hemisphere). Two additional screws were implanted for structural support of the head stage and for grounding. Teflon-coated braided stainless steel wire (A-M Systems, Sequim, WA, USA) was stripped at the tip and wrapped around the implanted screws. Two additional wires were stripped at the tips and implanted in the superficial muscles of the neck for EMG recordings of postural activity. All wires were crimped to amphenol pins (A-M Systems) and inserted into a plastic headstage (Plastics One). Implantable optical fibres (230 μm, numerical aperture 0.39; Thorlabs, Newton, NJ, USA) were constructed using published methods (Sparta *et al.* 2012) and stereotaxically directed into the ventrolateral medulla 0.5–0.8 mm dorsal to the LVV injection sites. The head stage and optical fibre–ferrule assemblies were secured to the skull using a two-part epoxy (Loctite, Henkel, Düsseldorf, Germany). Incisions were then closed in two layers (muscle and skin) with absorbable sutures and vet bond adhesive. Rats recovered for a minimum of 4 weeks before experiments were conducted. A subset of animals was then implanted with radiotelemetry probes (PA-C10; Datasciences International, Saint Paul, MN, USA) to record blood pressure (BP) from the descending aorta via the right femoral artery. Animals were left to recover for at least another week before physiological experiments began.

Physiological experiments in freely behaving rats

Rats were first habituated to the testing environment, which consisted of a Buxco unrestrained plethysmography chamber modified to allow tethered EEG/EMG recordings and optical stimulation. This equipment was visually isolated and placed in low ambient noise conditions. On the day of the experiment, rats were lightly anaesthetized with isoflurane (induction with 5%, maintenance with 2% in pure oxygen for $<$ 1 min) to permit cleaning of hardware and connections to the ferrule and EEG/EMG recording assembly. A 200 μm thick multimode optical fibre was terminated with a ferrule and mated to the implanted ferrule with a zirconia sleeve. Optical matching gel (Fibre Instrument Sales, Oriskany, NY, USA) was applied at the ferrule junction to minimize light loss. A minimum of 1 h was allowed for recovery from anaesthesia and the emergence of stable sleep patterns. Recordings were made between 12.00 and 18.00 h, over multiple days, with a minimum of 3 days' rest between tests. The ventilatory response to RTN photoinhibition or activation was assessed using barometric, unrestrained whole body plethysmography (EMKA Technologies, Falls Church, VA, USA). The plethysmography chamber was continuously flushed with 1.5 l min^{-1} of 21% O_2 balanced with N_2. Three or 6% CO_2 was added when required, leaving the oxygen percentage constant. Photoinhibition of RTN under hyperoxia (65% O_2 in

N_2) was also performed, as previously described (Basting *et al.* 2015). The gas composition was regulated by computer-driven mass flow controllers for O_2, N_2 and CO_2 (Alicat Scientific, Inc., Tucson, AZ, USA). Temperature and humidity within the plethysmography chamber were kept constant.

Optogenetics

Photoinhibition of Arch-expressing RTN neurons was achieved with a green laser (532 nm; Shanghai Laser and Optics Century, Shanghai, China). Photostimulation of ChR2-expressing RTN neurons was performed using a blue laser (473 nm; CrystaLaser, Reno, NV, USA). The lasers were controlled by TTL pulses from a Grass model S88 stimulator (AstroMed Inc., West Warwick, RI, USA). Continuous green light (∼5 mW) was applied bilaterally using a splitter through 200 μm thick multimode optical fibre (Thorlabs) in 10 s episodes of continuous illumination. This method effectively silences chemosensitive RTN neurons under anaesthesia (see fig. 2 in Basting *et al.* 2015). ChR2-transduced neurons were excited with pulses of blue light (5 ms, ∼9 mW) delivered at 20 Hz for 20 s (Kanbar *et al.* 2010; Abbott *et al.* 2013*a*; Burke *et al.* 2014) or intermittently to entrain the breathing cycle (four 5 ms long pulses, 50 ms interval delivered at a frequency greater than resting $f_{R,}$ see Abbott *et al.* 2011).

Data acquisition and analysis

Physiological signals were acquired and processed using Spike v7.03 software (CED Cambridge, UK). EEG and EMG were amplified and band pass filtered (EEG: 0.1–100 Hz, ×1000. EMG: 300–3000 Hz, ×1000) and acquired at a sampling frequency of 1 kHz. The signal generated by the differential pressure transducer connected to the plethysmography chamber was amplified and band pass filtered (0.1–15 Hz, ×100) and acquired at a sampling frequency of 1 kHz. The signal from the radiotelemetry probe was acquired at a sampling frequency of 0.2 kHz. Mean arterial pressure and heart rate (HR) were extracted from pulsatile BP recordings from the descending aorta based on values calibrated before implantation of the telemetry probe. Periods of non-REM sleep, REM sleep and quiet wake were classified based on EEG, EMG activity and the patterns of cardiovascular and breathing activity. During non-REM sleep, EEG spectra were dominated by delta activity (0.5–4 Hz), with little or no EMG activity and a stable breathing pattern, BP and HR. REM sleep was characterized by stable theta oscillations (6–8 Hz), neck muscle atonia, an irregular breathing pattern and bradycardia with BP fluctuations. Quiet wake was characterized by a reduction in total power with EMG tone and elevated HR. A minimum of six photoactivation trials were conducted in each rat in each state. Average breathing values were extracted from trials in non-REM sleep, REM sleep and quiet wake that were not contaminated by body movements, as indicated by EMG activity. Baseline values for all parameters were calculated from the 20 s before the photoactivation period. Respiratory frequency (f_R, breaths per min) and tidal volume (V_T, area under the curve during the inspiratory period calibrated to waveforms generated by injecting 5 ml of dry air from a syringe during the experiment, expressed in ml per 100 g body weight (BW)) were calculated using Spike software v7.3 (CED). These values were used to calculate minute ventilation ($V_E = f_R \times V_{T,}$ expressed as ml 100 g BW min^{-1}).

All data sets were tested for normality using the Shapiro–Wilk test, then differences within and between groups were determined using one- or two-way repeated measures (RM) ANOVA with Bonferroni multiple comparisons. Linear regression, Student's t test and non-parametric Kruskal–Wallis tests were also performed as required. All values are expressed as means ± SEM and significance indicated (one symbol, $P < 0.05$; two symbols, $P < 0.01$; three symbols, $P < 0.005$, four symbols, $P < 0.0001$).

Histology

Animals were deeply anaesthetized with sodium pentobarbital and perfused transcardially with 4% paraformaldehyde, brains removed and processed as described previously (Abbott *et al.* 2009; Burke *et al.* 2014). Immunohistochemistry with antibodies against tyrosine hydroxylase (sheep anti-TH, 1:2000; Millipore, Billerica, MA, USA), EYFP (chicken anti-GFP, 1:1000; AVES Labs, Tigard, OR, USA) or mCherry (rabbit anti-dsRed, 1:500, Clontech no. 632496; Clontech Laboratories, Mountain View, CA, USA) and Phox2b (rabbit anti-Phox2b, 1:8000, a gift from J.F. Brunet, Ecole Normale Superieure, Paris, France) were performed as previously described (Abbott *et al.* 2009; Burke *et al.* 2014). Cell mapping, counting and photography were done using the Neurolucida system (MicroBrightfield, Inc., Colchester, VT, USA) with a Zeiss Axioskop microscope with computer driven stage and Zeiss MRc camera. Cell counts were taken from a 1 in 6 series of 40 μm sections and only profiles containing a nucleus were counted.

Results

State dependence of the hypercapnic ventilatory reflex

Exposure to 3% F_{I,CO_2} did not detectably perturb natural sleep in any of the rats ($n = 10$). Most rats (seven of 10) were also able to cycle through periods of non-REM and REM sleep in the presence of 6% F_{I,CO_2} (Fig. 1).

During REM sleep, breathing was either regular or very labile (Figs 1, 4 and 6 and Supplemental Videos 3–4). The average f_R measured in REM sleep was higher than during non-REM sleep and quiet wake (n = 10; REM sleep: 93 ± 3 breaths min^{-1}; non-REM sleep: 74 ± 3; quiet wake: 77 ± 4; REM *vs.* non-REM, P = 0.0001; REM *vs.* wake, P = 0.0003; non-REM *vs.* wake, P = 0.2). V_T (ml breath 100 g^{-1}) was lower in REM sleep than non-REM sleep and quiet wake (n = 10; REM sleep: 0.32 ± 0.02; non-REM sleep: 0.41 ± 0.01; quiet wake: 0.44 ± 0.03; REM *vs.* non-REM, P = 0.003; REM *vs.* quiet wake, P = 0.002; non-REM *vs.* wake, P = 0.6). Minute ventilation ($V_E = f_R \times V_T$; ml min 100 g^{-1}) was virtually identical across the three states (n = 10; REM sleep: 30 ± 2; non-REM sleep: 30 ± 1; quiet wake: 34 ± 2; one-way RM ANOVA: $F_{2,14}$ = 2.969, P = 0.1).

Exposure to 3 and 6% F_{I,CO_2} during non-REM and quiet wake increased f_R, V_T and V_E linearly (Fig. 1*C–E*). During REM sleep, V_T also increased linearly with F_{I,CO_2} but f_R was invariant. The slopes of the linear regression between V_T and F_{I,CO_2} ($\Delta V_T/\Delta F_{I,CO_2}$ in ml 100 g^{-1}/1% F_{I,CO_2}) were not state-dependent (Fig. 1*D*; n = 7; REM sleep: 0.04 ± 0.004; non-REM sleep: 0.05 ± 0.009; wake: 0.06 ± 0.009; One-way RM ANOVA: $F_{2,10}$ = 3.537,

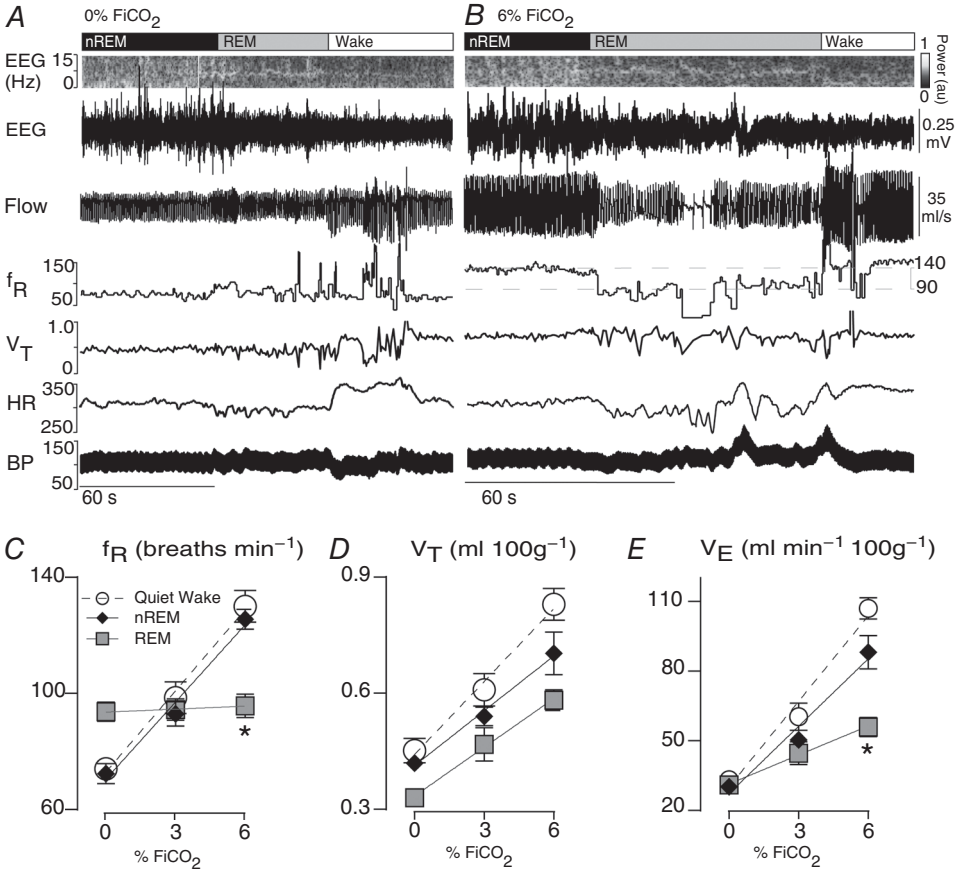

Figure 1. State dependence of the hypercapnic ventilatory reflex in rat
A, breathing and cardiovascular function at rest. Shown from top to bottom: EEG power spectrum (0–15 Hz), EEG (raw signal), air flow signal (plethysmography, inspiration downward), f_R (breaths min^{-1}), V_T (ml 100 g^{-1}), HR (beats min^{-1}) and BP (telemetric recording, mmHg). During non-REM sleep, EEG power was concentrated within the delta range (0.5–4 Hz), REM sleep was identified by a strong concentration of power in the 6–8 Hz range (theta) and quiet wake by a large reduction in total power (desynchronized state). Breathing during REM sleep was faster, more labile and shallower than during non-REM sleep. Bradycardia and BP fluctuations also commonly occurred in REM sleep, the result of co-activation of cardiac vagal and sympathetic vasomotor outflows by central command with impaired baroreflex function. *B*, breathing and cardiovascular function in hypercapnia (6% F_{I,CO_2}; same rat as in *A*). V_T and f_R were markedly increased in non-REM sleep or wake. Transition from non-REM sleep into REM sleep caused an abrupt reduction in breathing rate that was reversed at the transition to wake (hatched horizontal lines denote the ∼50 breaths min^{-1} reduction in f_R during REM sleep in this example). No differences in BP and HR regulation were observed under hypercapnia. *C–E*, f_R, V_T and V_E at 0%, 3% and 6% F_{I,CO_2} measured across sleep–wake states (n = 7). ∗Gain (slope of linear regressions) significantly different during REM *vs.* both quiet wake (P = 0.0001) and REM sleep (P = 0.004; see Results section for detailed statistics). BP, blood pressure; HR, heart rate; nREM, non-REM.

$P = 0.07$). However, during REM sleep, f_R was unaffected by CO_2 ($n = 7$; 0% F_{I,CO_2}: 94 ± 3 bpm; 3% F_{I,CO_2}: 94 ± 4; 6% F_{I,CO_2}: 96 ± 4; one-way RM ANOVA: $F_{2,12} = 0.1934$, $P = 0.8$). Accordingly, the slopes of the linear regressions between f_R and F_{I,CO_2} ($\Delta f_R/\Delta F_{I,CO_2}$ in breaths min^{-1}/1% F_{I,CO_2}) were markedly different (Fig. 1*C*; $n = 7$; REM sleep: 0.3 ± 0.5; non-REM sleep: 8.9 ± 0.7; quiet wake: 9.3 ± 1.2; REM *vs.* non-REM, $P < 0.0001$; REM *vs.* quiet wake, $P = 0.001$; non-REM sleep *vs.* quiet wake, $P > 0.9$). Finally, the slopes of the regressions between V_E and F_{I,CO_2} ($\Delta V_E/\Delta F_{I,CO_2}$ in ml min 100 g/1% F_{I,CO_2}) were also different during REM sleep *vs.* the other states (Fig. 1*E*; $n = 7$; REM sleep: 4.2 ± 0.6; non-REM sleep: 9.7 ± 1.2; wake: 12.3 ± 0.6; REM *vs.* non-REM, $P < 0.004$; REM *vs.* wake, $P < 0.0001$; non-REM *vs.* wake, $P = 0.05$).

In summary, in rats, f_R is no longer under chemoreceptor control during REM sleep but the tidal volume component of the HCVR has approximately the same gain during all states.

Optogenetic inhibition of retrotrapezoid nucleus neurons in REM sleep reduces V_T selectively

Arch was photoactivated in 10 s episodes during established periods of non-REM sleep, REM sleep or quiet wake. During non-REM sleep and quiet wake, Arch-mediated neuronal inhibition reduced both f_R and V_T whereas during REM sleep Arch activation reduced V_T but did not change f_R (Fig. 2*A–D*) ($n = 8$; f_R (baseline *vs.* Arch activation): non-REM sleep, $P < 0.0001$, REM sleep, $P > 0.9$, wake, $P < 0.0001$; V_T (baseline *vs.* Arch activation): non-REM sleep, $P < 0.0001$; REM sleep, $P = 0.001$, wake, $P < 0.0001$; V_E (baseline *vs.* Arch activation): non-REM, $P < 0.0001$; REM, $P = 0.006$; wake, $P < 0.0001$).

We also performed these experiments under hyperoxia (65% F_{I,O_2}; same eight rats), which silences the carotid bodies (Dejours, 1962; Gonzalez *et al.* 1994). As found previously (Basting *et al.* 2015), during non-REM sleep and quiet wake, Arch activation produced a much larger reduction of f_R and V_T than under normoxia (group data in Fig. 2*E*, representative example in Fig. 3 with corresponding Supplemental Videos 1–2). However, during REM sleep, again, Arch activation reduced V_T but had no effect on f_R (group data in Fig. 2*E*, representative example in Fig. 4 and corresponding Videos 3–4) [$n = 8$; f_R (baseline *vs.* Arch activation): non-REM, $P < 0.0001$; REM, $P > 0.9$; wake, $P < 0.0001$. V_T (baseline *vs.* Arch activation): non-REM, $P = 0.0001$; REM, $P = 0.009$; wake, $P = 0.0001$. V_E (baseline *vs.* Arch activation): non-REM, $P < 0.0001$; REM, $P = 0.04$; wake, $P < 0.0001$].

BP and HR were unaffected by photoactivation with green light (Fig. 2*A–C*, Table 1).

Retrotrapezoid nucleus activation in REM sleep increases V_T but not f_R

ChR2-transduced neurons were photoactivated (5 ms pulses, 20 Hz, 20 s episodes) during non-REM sleep, REM sleep and quiet wake. ChR2-mediated stimulation increased both f_R and V_T during non-REM sleep and quiet wake (Fig. 5*A*, *C* and *D*). In REM sleep, V_T increased but f_R did not change (Fig. 5*B* and *D*) [$n = 10$; f_R (baseline *vs.* ChR2 stimulation): non-REM, $P < 0.0001$; REM, $P = 0.6$; quiet wake, $P < 0.0001$; V_T (baseline *vs.* ChR2-stimulation: non-REM, $P < 0.0001$; REM, $P = 0.0003$; quiet wake, $P < 0.0002$].

BP and HR were unchanged by the photostimulus (Fig. 5*A–C*, Table 1).

Phasic retrotrapezoid nucleus stimulation does not entrain breathing during REM sleep and does not produce active expiration during either form of sleep

As reported before (Abbott *et al.* 2011), short light trains (3–4 pulses per train, 20 Hz, 2–5 ms pulses) applied at frequencies above resting f_R entrained the breathing cycle (range: 66–108 breaths min^{-1}; Fig. 6*A*). However, we found that pacing could be produced during non-REM sleep and quiet wake but never during REM sleep (Fig. 6*A–D*).

In the absence of RTN stimulation, peak expiratory flow occurred in early expiration (E1) when the rats were awake or in non-REM sleep. This pattern persisted during phasic RTN photostimulation when the rats were in non-REM or REM sleep (Fig. 6*B* and *E*). However, during quiet wake, the same RTN stimuli reduced E1 expiratory flow and produced a strong late expiratory flow (E2) signal indicative of active (abdominal) expiration (Fig. 6*B*; black arrows). This pattern of breathing is better appreciated by examining stimulus-triggered averages of the plethysmography signal (Figs 6*E* and 7*A* and *B*). In five of nine rats, a single large peak expiratory flow occurred during this late expiratory phase (Fig. 7*C*). The remainder of the rats displayed a biphasic expiratory flow as per (Abbott *et al.* 2011). We divided the expiratory phase in two segments (E1 and E2) corresponding to each of the two peak expiratory flows and measured the expiratory airflow volume occurring in each phase at rest and during phasic RTN stimulation. In quiet wake, the volume of E1 expiratory airflow at rest was 0.38 ± 0.02 ml 100 g^{-1} and decreased with RTN stimuli to 0.25 ± 0.01 ml 100 g^{-1} (Fig. 7*D*; $n = 9$; two-way ANOVA with Bonferroni's multiple comparisons: Wake (rest) *vs.* Wake (laser), $P = 0.0005$). Conversely, E2 expiratory airflow at rest was 0.14 ± 0.01 ml 100 g^{-1} and increased with

RTN stimuli to 0.25 ± 0.02 ml 100 g^{-1} ($P = 0.0001$). There was no change in the relative E1 and E2 expiratory volume under resting conditions, nor with phasic RTN stimuli during non-REM sleep (Fig. 7*D*); total expiratory airflow (volume of E1 + E2) did not differ between any groups (Fig. 7*D*).

In summary, phasic RTN stimulation at frequencies above resting f_R entrained the breathing cycle. The trajectory of the expiratory flow was detectably altered only when the animals were awake. Under these circumstances, expiratory flow slowed during the early post-inspiratory phase and was strongly enhanced during the late expiratory phase.

During retrotrapezoid nucleus-imposed pacing, selective reduction of the post-inspiratory phase accounts for the reduction of breathing cycle length

Phasic RTN stimulation entrained breathing equally during non-REM sleep and quiet wake (Fig. 8*A* and *B*, see also Fig. 6*C*). As previously observed, the light stimuli always settled in the mid- to late-expiratory phase (Potts *et al.* 2005; Abbott *et al.* 2011; Pagliardini *et al.* 2011). During non-REM sleep, pacing shortened the expiratory phase (Fig. 8*C*; $n = 8$; Kruskal–Wallis $H = 41.93$, $P < 0.0001$) without changing the inspiratory duration (Fig. 8*C*; Kruskal–Wallis $H = 7.027$, $P = 0.4$).

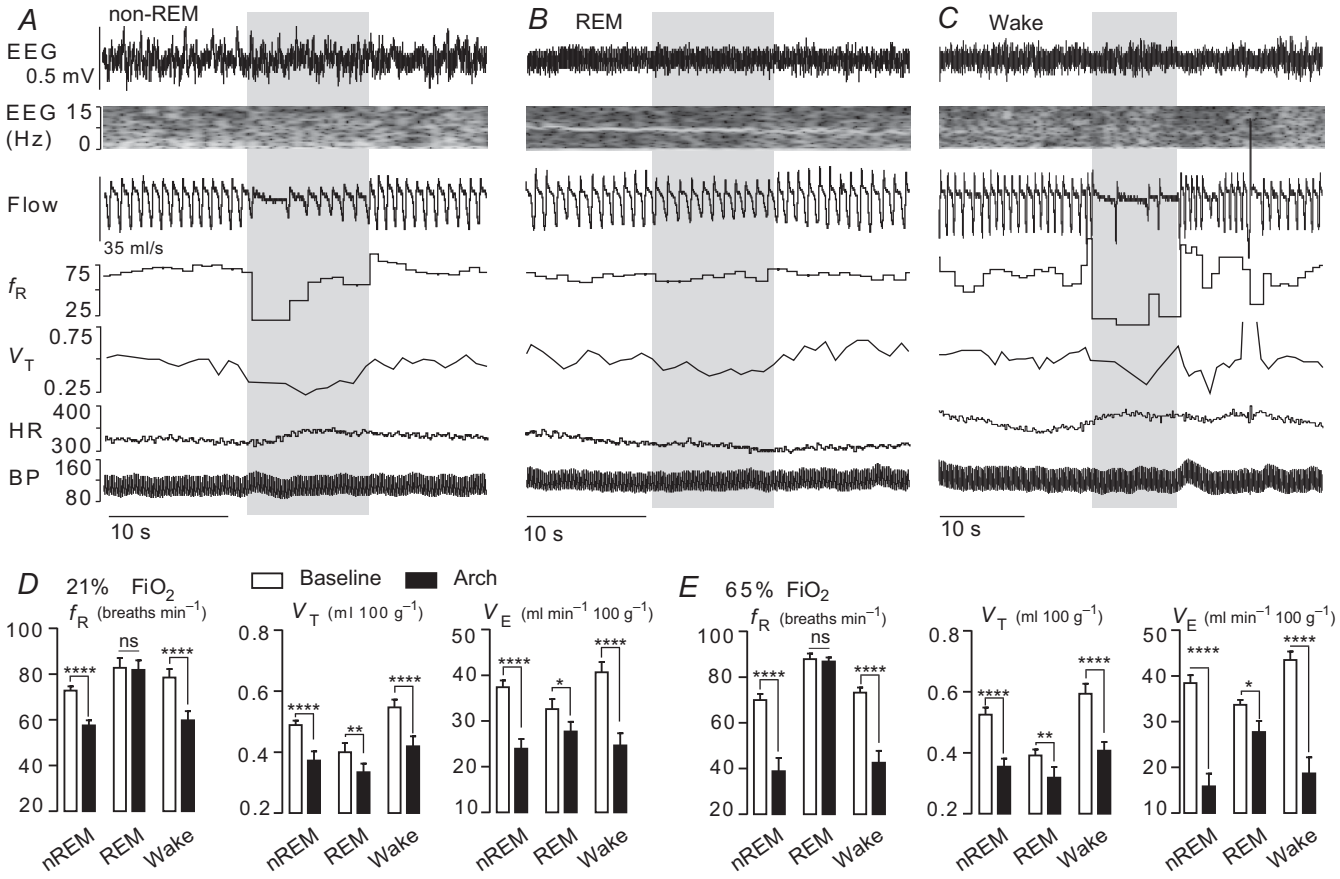

Figure 2. State dependence of the breathing changes evoked by retrotrapezoid nucleus inhibition
A–C, hypoventilation caused by bilateral Arch activation (10 s) in one rat at 21% F_{I,O_2} in non-REM sleep (*A*), REM sleep (*B*) and quiet wake (*C*). Arch activation decreased V_T in all three states, decreased f_R during non-REM sleep and quiet wake but did not change f_R during REM sleep. Arch activation did not change BP, HR or sleep state. *D*, ventilation parameters at rest and during Arch activation in normoxia (21% F_{I,O_2}; $n = 8$). *E*, ventilation parameters at rest and during Arch activation in hyperoxia (65% F_{I,O_2}; $n = 8$). The effects of Arch activation on ventilation were amplified in hyperoxia but qualitatively the same as in normoxia. In REM sleep, Arch activation had no effect on f_R. Arch activation reduced V_T under all conditions. Refer to online data supplement for video examples of Arch activation in hyperoxia. Significance (baseline *vs.* Arch stimulation; two-way repeated measures ANOVA with Bonferroni's correction for multiple comparisons): $^*P < 0.05$, $^{**}P < 0.01$, $^{***}P < 0.005$, $^{****}P < 0.001$. BP, blood pressure; HR, heart rate; nREM, non-REM.

Table 1. Blood pressure and HR at rest or during Arch or ChR2 photostimulation

State	Non-REM sleep		REM sleep		Quiet wake	
Variable	**Rest**	**Arch**	**Rest**	**Arch**	**Rest**	**Arch**
n	5	5	4	4	5	5
MAP (mmHg)	109 ± 4	108 ± 4	119 ± 2	117 ± 2	115 ± 6	113 ± 5
HR (bpm)	300 ± 9	300 ± 9	289 ± 6	287 ± 9	310 ± 8	311 ± 8
Variable	**Rest**	**ChR2**	**Rest**	**ChR2**	**Rest**	**ChR2**
n	7	7	7	7	7	7
MAP (mmHg)	109 ± 3	106 ± 3	114 ± 4	113 ± 4	109 ± 4	108 ± 3
HR (bpm)	306 ± 7	315 ± 8	298 ± 6	304 ± 5	314 ± 12	313 ± 12

Abbreviations: HR, heart rate; MAP, mean arterial blood pressure.
Telemetric blood pressure and HR recordings in rats habituated to the plethysmography chamber during various states of vigilance. No change in resting MAP or HR was observed during photostimulation of Arch$^+$ or ChR2$^+$ rats. Statistics: two-way ANOVA.

During wake, the post-inspiratory phase (E1) could be clearly distinguished from the active expiratory phase (E2). Pacing shortened the E1 phase (Fig. 8*D*; $n = 7$; Kruskal–Wallis $H = 23.76$, $P = 0.001$) without altering the E2 phase (Kruskal–Wallis $H = 3.962$, $P = 0.8$) nor inspiratory duration (Kruskal–Wallis $H = 3.510$, $P = 0.8$).

Histology

The ChR2-transduced neurons (mCherry-positive, mCherry detection enhanced by immunohistochemistry) were located under the facial motor nucleus within the rostral half of RTN (Fig. 9*Aa* and *Ab*)(Fig. 9

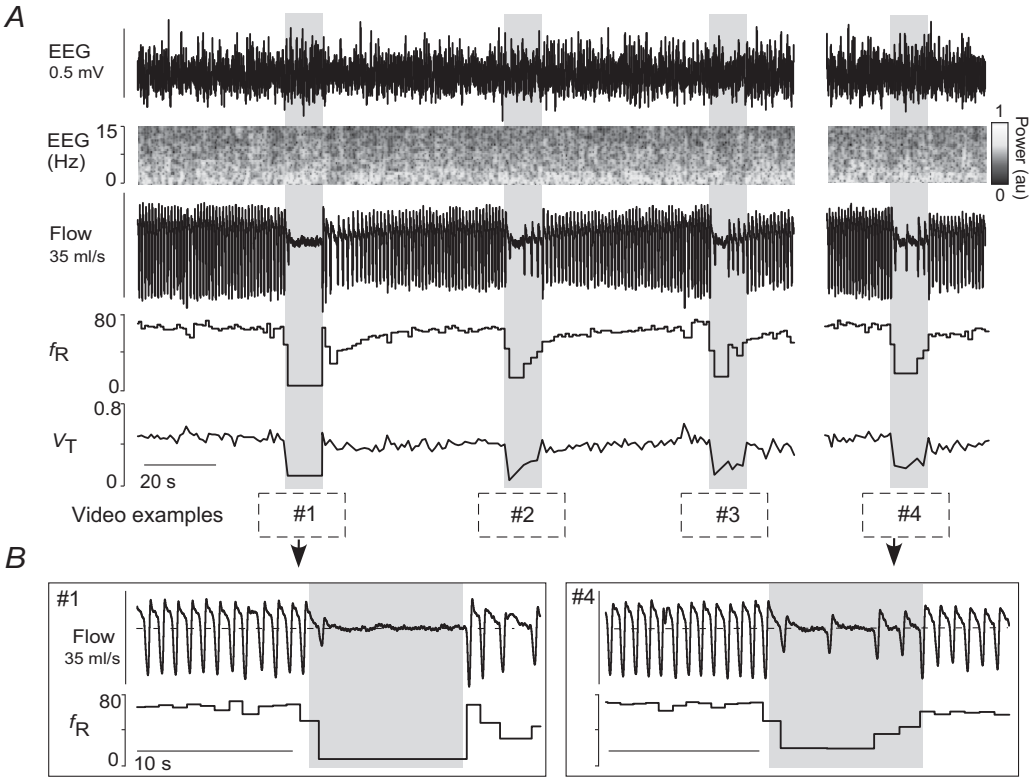

Figure 3. Retrotrapezoid nucleus inhibition during non-REM sleep in hyperoxia
A, profound hypoventilation caused by bilateral Arch activation (10 s; grey rectangles) in one rat at 65% F_{I,O_2} in non-REM sleep. Despite this sudden hypoventilation, the animal does not arouse from non-REM sleep (EEG delta wave activity: 0.5–4 Hz). Traces correspond to the four examples shown in Supplemental videos 1–2. *B*, enlarged traces of trials 1 and 4.

(Takakura *et al.* 2008). The number of transduced RTN neurons (TH-negative) counted (1:6 series of coronal sections) was 32 ± 5 per rat (n = 8). These sections also contained 27 ± 7 catecholaminergic neurons judged to be A5 noradrenergic neurons rather than C1 adrenergic neurons based on location. RTN contains approximately 2000 neurons in rats (Takakura *et al.* 2008). On average, only 10% (range 5–18%) were therefore transduced.

The distribution of Arch-transduced (EYFP-immunoreactive) neurons was comparable (though bilateral) and centred on the caudal rather than rostral half of RTN (Fig. 9*Ba* and *Bb*)(Fig. 9. We identified 77 ± 15 Arch-transduced RTN neurons ($EYFP^+/TH^-/Phox2b^+$) and 97 ± 10 catecholaminergic, probably C1, neurons in a one in six series of transverse sections (n = 8). Thus, 23% of RTN CRCs (range 20–42%) were detectably transduced with Arch (6 × 77/2000).

Green laser light control experiments

To control for possible non-selective effects of continuous application of green light, the light was delivered in 10 s episodes bilaterally to the RTN of 5 rats that had received injections of vector but in which transduced neurons were not detected postmortem ($Arch^-$ rats; n = 5). The location of the optical fibre tips was recorded for both $Arch^-$ (n = 5) and $Arch^+$ rats (n = 8). The optic fibre tips were positioned in the same region of the ventrolateral medulla oblongata in both rat groups, mostly dorsal to the RTN neurons (Fig. 10*A*). Light delivery during non-REM sleep or quiet wake had no effect on breathing in $Arch^-$ rats (Fig. 10*B* and *C*).

Discussion

We report two new findings. First, the respiratory drive contributed by RTN has the same state dependency as the HCVR. Specifically, like CO_2, RTN regulates f_R and V_T during wake and non-REM sleep whereas, during REM sleep, neither RTN nor CO_2 exert any control over f_R. Second, RTN stimulation reduces post-inspiratory (E1) airflow and elicits active E2 expiration but this pattern is observed only during wake.

Loss of f_R control contributes to reduced chemoreflex gain during REM sleep

As reported before (Fagenholz *et al.* 1976; Sullivan *et al.* 1979; Coote, 1982; Douglas *et al.* 1982*a*; Douglas *et al.* 1982*b*; Berthon-Jones & Sullivan, 1984; Smith *et al.* 1997; Horner *et al.* 2002), the HCVR was similar during non-REM sleep and quiet wake but significantly reduced during REM sleep. We also confirm that hypercapnia

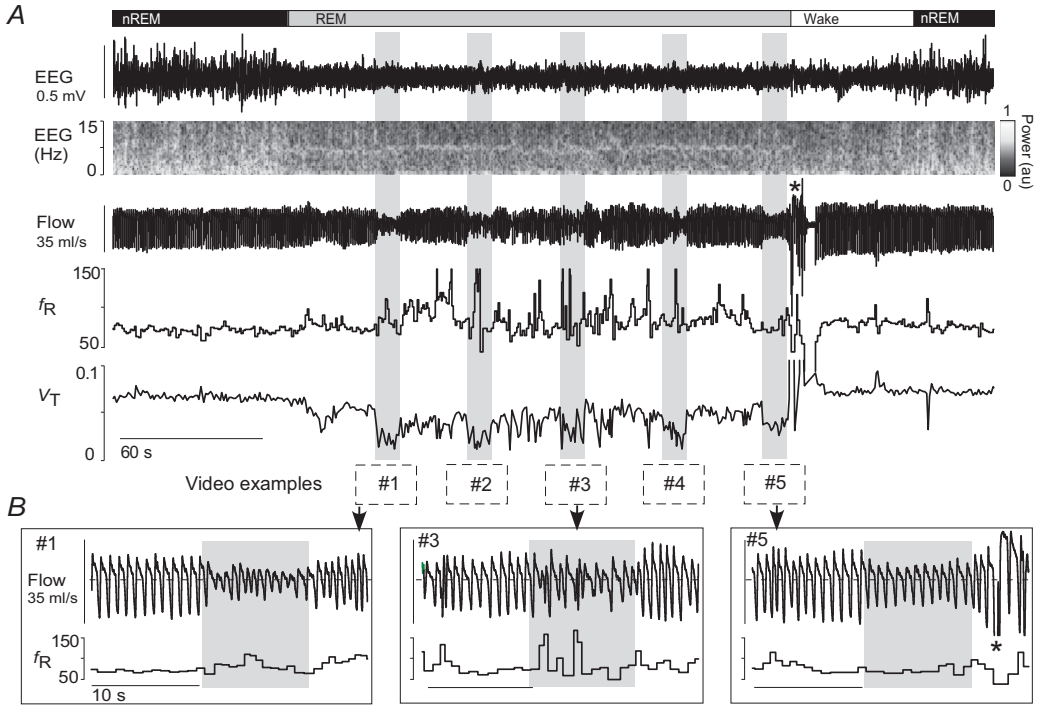

Figure 4. Retrotrapezoid nucleus inhibition during REM sleep in hyperoxia
A, bilateral Arch activation (10 s; grey rectangles) in one rat at 65% F_{I,O_2} in REM sleep decreased V_T in all trials, but did not reduce f_R (same animal as Fig. 3). Traces correspond to the five examples in the Supplemental videos 3–4. *B*, enlarged traces of trials 1, 3 and 5. Animal awoke from REM sleep 3 s after the fifth trial (asterisk) then returned to non-REM sleep. nREM, non-REM.

does not change f_R during REM sleep (Berthon-Jones & Sullivan, 1984; Horner *et al.* 2002; Nakamura *et al.* 2007). By contrast, hypercapnia reportedly produces comparable increases in diaphragmatic EMG and V_T across wake, non-REM and REM sleep states (Haxhiu *et al.* 1987; Horner *et al.* 2002; Nakamura *et al.* 2007). Consistent with these observations, a given increment of F_{I,CO_2} produced a similar V_T increase during wake, non-REM sleep and REM sleep in our experiments.

In short, the HCVR persists during REM sleep but with reduced gain because this reflex operates only via changes in V_T. This characteristic seems present in all mammals, including humans. Its impact on the HCVR gain is presumably larger in species such as rodents in which f_R stimulation contributes most to the reflex. As is the case during REM sleep, homeostatic control of P_{CO_2} via changes in V_T persists during voluntary breathing (Haouzi & Bell, 2009; Ohashi *et al.* 2013).

Inability of retrotrapezoid nucleus to regulate f_R contributes to reduced chemoreflex during REM sleep

In rats, the breathing pattern in REM sleep alternates between periods during which f_R is increased but remains fairly regular, or increased with periods of marked breathing lability. In neither phase could we modify f_R by stimulating or inhibiting RTN. Thus the inability of RTN neurons to control f_R underlies, partly at least, the loss of chemoreceptor control over f_R during REM sleep. Our observations also rule out the hypothesis that RTN could be mediating the tachypnoea occurring during REM sleep (Fraigne & Orem, 2011).

Two possibilities could explain RTN's inability to regulate f_R during REM sleep: (a) RTN could be silent or unexcitable, or (b) this nucleus could remain active and CO_2 responsive but its effect on the rhythm generator could be gated out downstream. Although RTN neurons

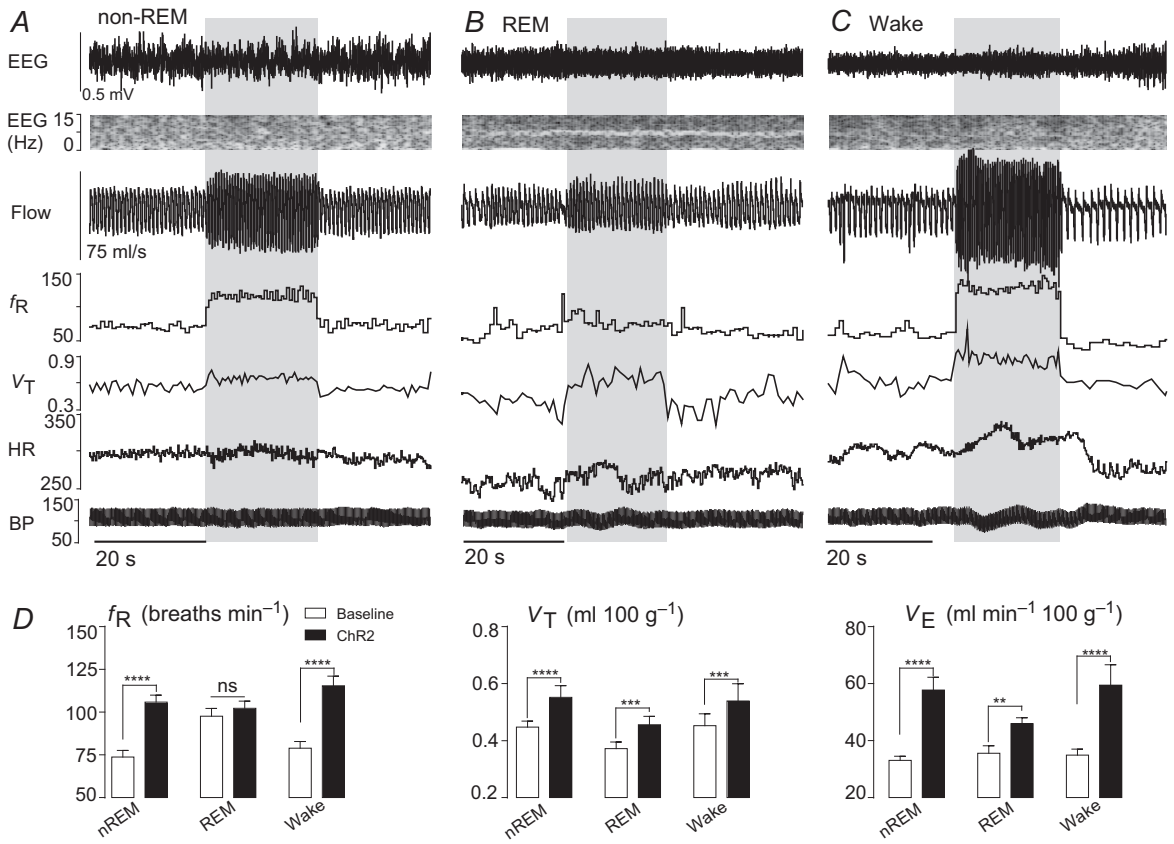

Figure 5. State dependence of the breathing changes evoked by rostral retrotrapezoid nucleus stimulation
A–C, hyperventilation evoked by unilateral ChR2 activation (20 s, blue bar) in one rat at 21% F_{I,O_2} in non-REM sleep (*A*), REM sleep (*B*) and quiet wake (*C*). ChR2 activation increased V_T in all three states, increased f_R in non-REM and quiet wake states but had no effect on f_R during REM sleep. ChR2 activation had little effect on BP and did not produce arousal from sleep. *D*, ventilation parameters at rest and during ChR2 activation in rats across sleep–wake states in normoxia ($n = 10$). Significance (baseline *vs.* Arch stimulation; two-way repeated measures ANOVA with Bonferroni's correction for multiple comparisons): $^{**}P < 0.01$, $^{***}P < 0.005$, $^{****}P < 0.001$. BP, blood pressure; HR, heart rate; nREM, non-REM.

are mildly activated by serotonin, a transmitter whose release presumably decreases during REM sleep in this brain region as elsewhere (Veasey *et al.* 1995; Mulkey *et al.* 2007), the first interpretation (a) is the least plausible. First, optogenetic activation of RTN or hypercapnia still increased V_T during REM sleep indicating that RTN does remain excitable. Even if distinct subtypes of RTN neurons regulated f_R *vs.* V_T it seems unlikely that only the

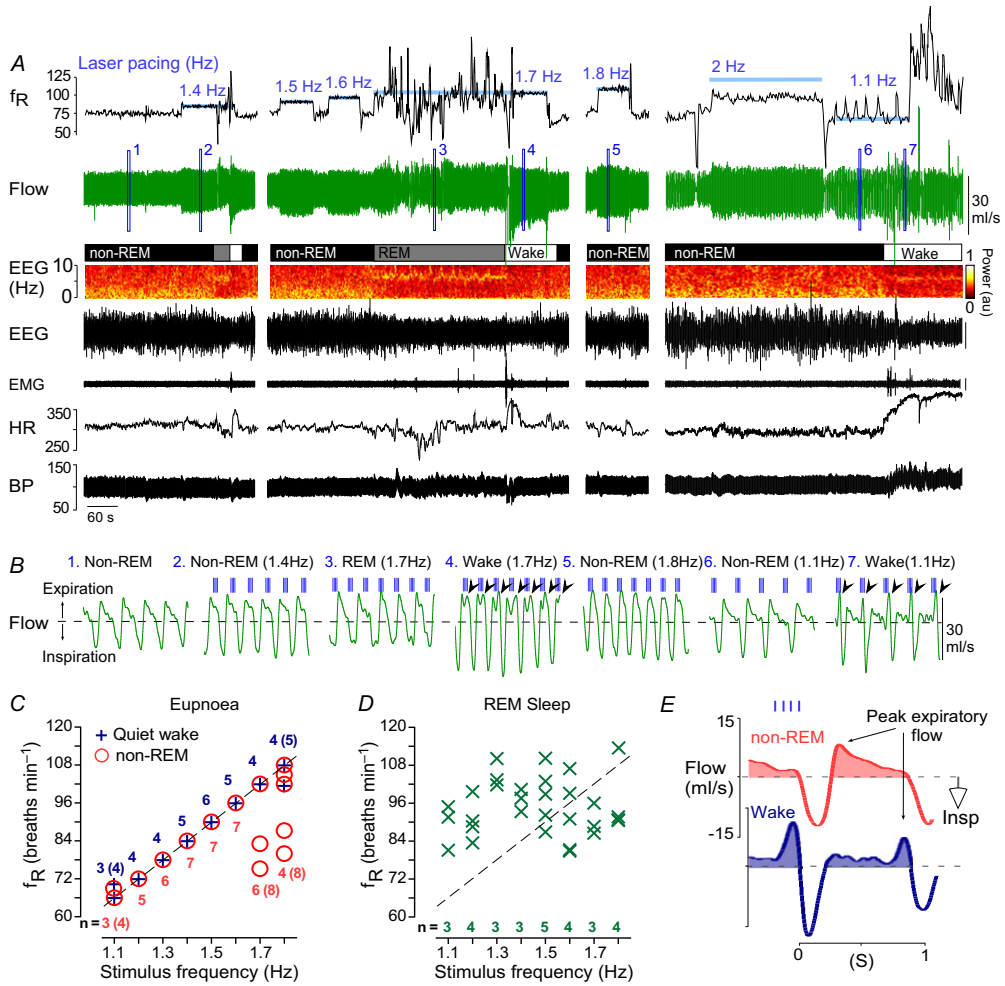

Figure 6. Breathing entrainment by RTN stimulation is state-dependent.
A, example of breathing entrainment elicited by photostimulation of RTN (trains of 4 × 3 ms light pulses at 20 Hz; stimulation at blue bars in f_R trace). Faithful entrainment (f_R = train frequency) in the range of 66–108 breaths min^{-1} (1.1–1.8 Hz) was obtained during non-REM sleep and wake but entrainment failed at 2 Hz. During REM sleep, no entrainment was produced. *B*, expanded plethysmography flow signals (light pulses delivered at vertical blue lines above flow traces; excerpts 1–7 taken from where indicated in the flow trace of *A*). During entrainment, the light pulses 'settled' spontaneously during late to mid expiration. Note that during non-REM sleep peak expiratory flow at rest (no. 1) or during entrainment (nos 2, 5–6) occurs in early expiration. However, in wake, RTN stimulation produced a switch in peak expiratory flow to the late expiratory phase (arrowheads in excerpts 4 and 7), indicative of active expiration (Abbott *et al.* 2011; Pagliardini *et al.* 2011). *C*, group data from 11 animals showing the relationship between stimulus train frequency and f_R during non-REM sleep and wake states. Breathing was faithfully entrained between 1.2–1.6 Hz in all animals (single symbol for all animals); incomplete or unsuccessful entrainment outside this range is indicated by the individual symbols. Adjacent numbers are the number of animals that were successfully entrained at a given stimulation frequency (bracketed numbers indicate total rat number, including unsuccessful trials). Not every frequency was tested in every animal in each sleep–wake state; hence, the varying number of determinations for each tested frequency. *D*, group data during REM sleep (same rats as in *C*). There was no relationship between the stimulus train frequency and f_R. *E*, laser light-triggered waveform averages of the respiratory flow signal during entrainment at 1.1 Hz (light pulses in sky blue) in non-REM sleep (red) and wake (deep blue) with the shaded regions denoting the expiratory flow. In this example, RTN stimulation switched peak expiratory flow from early expiration in non-REM sleep to late expiration (active expiration) in wake. BP, blood pressure; HR, heart rate; Insp, inspiration; RTN, retrotrapezoid nucleus.

former would become unresponsive to ChR2 activation during REM sleep. Second, optogenetic inhibition of RTN inhibited V_T similarly during wake, non-REM and REM sleep indicating that these neurons remain active at rest during REM sleep. Accordingly, a more plausible explanation is that, during REM sleep, neither RTN nor CO_2 controls f_R because the respiratory rhythm generator is unresponsive to chemoreceptor input.

State-dependent control of active expiration by retrotrapezoid nucleus

Active expiration (Janczewski & Feldman, 2006; Feldman *et al.* 2013), can be elicited by activating RTN and surrounding catecholamine (CA) neurons in conscious rats (Abbott *et al.* 2011; and present results). In the *in situ* working heart–brainstem preparation in which lumbar expiratory activity persists at rest, this outflow is eliminated by inhibiting the same neuronal mix (Marina *et al.* 2010). The present study adds three novel elements. First, active expiration is elicited by stimulating the rostral portion of RTN, which contains hypercapnia-activated neurons but no C1 cells (Takakura *et al.* 2008). Thus, C1 cell stimulation is not required to produce active expiration. Second, RTN stimulation causes active expiration only when the rats are awake. Third, we suggest that upper airways resistance increases in parallel with active expiration, as denoted by the significant reduction in early expiratory (E1) airflow and the proportional increase in late expiratory (E2) airflow. In sum, we show that, along with active expiration, RTN stimulation produces a brief wake state-dependent facilitation of glottis closure immediately after inspiration to maintain expiratory lung volume, presumably for increased gas exchange. Thus, RTN stimulation appears capable of increasing alveolar ventilation via at least four mechanisms: increased inspiratory tidal volume; increased f_R; brief retention of inspired air during the early expiratory phase; and active expiration. According to the present results, the latter two mechanisms operate only during the waking state. However, we do not exclude the possibility that active expiration could be triggered even during non-REM sleep by stimulating a larger fraction of RTN neurons than in the present study.

Components of the circuitry responsible for active expiration (expiratory rhythm generator) overlap anatomically with the caudal RTN (Pagliardini *et al.* 2011; Feldman *et al.* 2013; Tupal *et al.* 2014). As shown

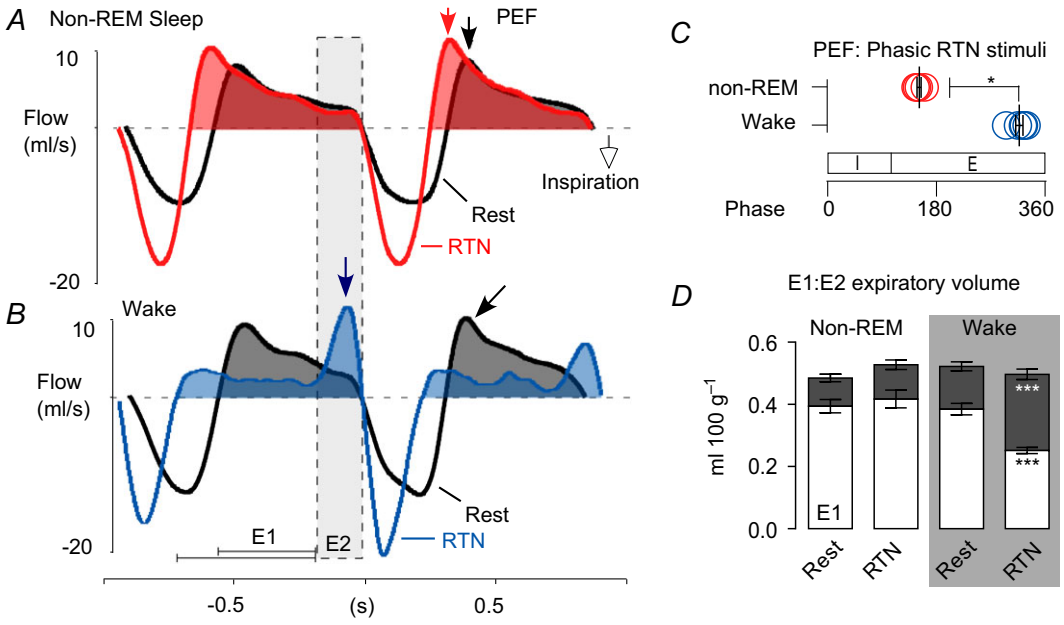

Figure 7. Wake state-dependent control of active expiration and upper airways resistance by the RTN
A and *B*, event-triggered waveform averages of the plethysmography signal at rest (black trace) and during phasic RTN stimulation (colour trace) in one rat during non-REM sleep (*A*) or quiet wake (*B*). Arrows point to PEF. In non-REM sleep (*A*) PEF occurred in early expiration (E1) regardless of whether RTN was activated or not. In the wake state (*B*) PEF shifted from early to late expiration (E2; active expiration) during RTN stimulation and early expiratory flow (E1 phase) was markedly reduced, presumably due to increased upper airway resistance. *C*, relationship between peak expiratory flow and the respiratory cycle with RTN stimulation during non-REM and quiet wake states. $n = 5$. Mann–Whitney non-parametric test. $^*P = 0.02$. *D*, expiratory airflow during early (E1; unfilled) and late (E2; grey fill) expiratory phases at rest or during phasic RTN stimuli in non-REM sleep or quiet wake. $n = 9$. Two-way ANOVA with Bonferroni's multiple comparison test. $^{***}P < 0.0005$. E, expiration; I, inspiration; PEF, peak expiratory airflow; RTN, retrotrapezoid nucleus.

here, active expiration can be triggered by stimulating RTN neurons located rostral to this region (Pagliardini *et al.* 2011; Feldman *et al.* 2013). Thus RTN, as defined in this laboratory ($Phox2b^+/VGLUT2^+/NK1R^+$ neurons located ventral to the facial motor nucleus) (Guyenet & Mulkey, 2010), can activate this oscillator but is probably not part of it. Consistent with this interpretation, RTN stimulation elicits active expiration only during wake whereas the same neurons increase f_R and inspiratory amplitude equally during non-REM sleep and quiet wake; the same reasoning applies for the effects of RTN on post-inspiratory airflow. The fact that RTN can only facilitate active expiration or laryngeal adduction during wake signifies that, in the absence of exercise, the recruitment of these muscles for breathing requires both a high level of CRC activation and a heightened network excitability presumably conferred by wake-ON neuromodulators (e.g. serotonin, noradrenaline, orexin) (Doi & Ramirez, 2008).

RTN innervates all the respiratory pattern generator (RPG) regions that harbour excitatory pump premotor neurons (Ballantyne & Richter, 1986; Dobbins & Feldman, 1994; Yokota *et al.* 2007; Bochorishvili *et al.* 2012). The excitatory input from RTN plausibly increases V_T by enhancing the discharges of these premotor cells. Phrenic motor neurons remain active regardless of the state of vigilance hence the relative state independence of the control of inspiratory amplitude by RTN and other chemoreceptors. By contrast, the activity of lumbar and other expiratory pump muscles is highly state-dependent, like that of other postural muscles or the musculature regulating upper airway resistance. This characteristic probably explains why RTN stimulates active expiration only during wake. Reductions of the activity of serotonin, noradrenaline and orexin neurons probably contribute to the reduced excitability of expiratory motor neurons or their cognate premotor inputs during sleep (Doi & Ramirez, 2008; Horner, 2009; Saper *et al.* 2010).

Expiratory airflow is regulated by upper airway resistance. The reduced E1 airflow with phasic RTN stimulation is probably a facilitation of glottic adduction by laryngeal constrictor (LC) muscles. The post-inspiratory activity of LC motor neurons could be enhanced by the polysynaptic drive via the Kolliker Fuse, a major target of RTN (Dutschmann & Herbert, 2006; Bochorishvili *et al.* 2012), and/or a network effect that augments phasic inspiratory inhibition of LC motor

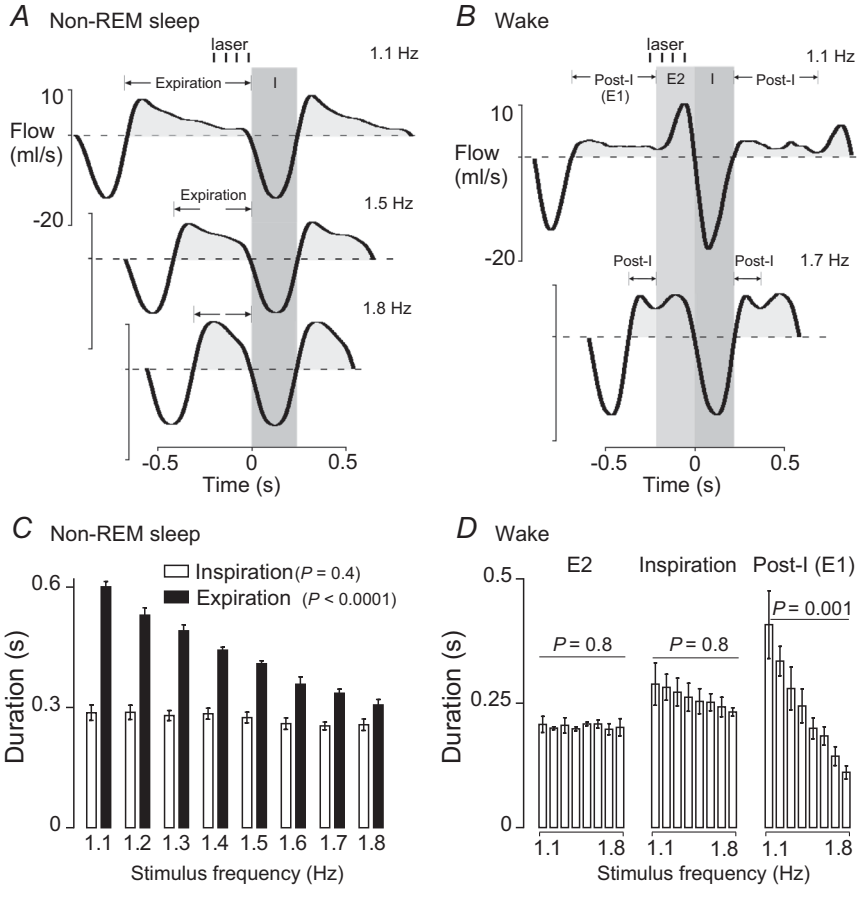

Figure 8. Phasic retrotrapezoid nucleus stimulation selectively shortens the post-inspiratory phase
A and *B*, event-triggered waveform averages of the plethysmography signal during light-induced breathing entrainment in one rat during non-REM sleep (*A*) and during quiet wake (*B*). ChR2-transduced retrotrapezoid nucleus neurons were photostimulated with trains of 4 × 3 ms long light pulses (20 Hz; represented as vertical blue bars) delivered at various frequencies between 1.1 and 18 Hz. Active expiration (large flow signal immediately preceding inspiration) was observed only during quiet wake periods. During non-REM sleep we measured only the I and E phases. During quiet wake, the duration of the late expiratory flow peak was defined as the E2 phase and the post-inspiratory phase (E1) represents the balance of the expiratory duration. *C* and *D*, group data from eight animals. Effect of stimulation frequency on the various phases of the breathing cycle evaluated using unpaired, non-parametric one-way ANOVA (Kruskal–Wallis). E, expiration; I, inspiration.

neurons and strengthens their post-inhibitory rebound (Sun *et al.* 2008; Bautista *et al.* 2010).

Retrotrapezoid nucleus stimulation selectively shortens the post-inspiratory phase

During quiet wake, phasic RTN stimulation increased f_R strictly by shortening the post-inspiratory (E1) phase. *In vitro*, somatic afferent stimulation also produces tachypnoea in this manner (Potts *et al.* 2005). In this case, the tachypnoea is attributed to disinhibition of the rhythmogenic pre-inspiratory/inspiratory (preI/I) neurons of the pre-Bötzinger complex as follows (Potts *et al.* 2005; Smith *et al.* 2013): activation of inhibitory E2 Bötzinger neurons by somatic afferents would cause early termination of E1 inhibitory neurons and, consequently, earlier depolarization of the preI/I neurons (Potts *et al.* 2005). RTN neurons could produce tachypnoea via this mechanism because they are excitatory and innervate the Bötzinger region (Mulkey *et al.* 2004; Bochorishvili *et al.* 2012). However, RTN neurons also project heavily to the pre-Bötzinger complex, including to the NK1 receptor expressing neurons that are suspected to include the preI/I cells (Gray *et al.* 1999; Bochorishvili *et al.* 2012). An excitatory input from RTN to these cells should also theoretically be able to reduce the duration of their inhibition during E1, allowing their burst discharges to occur earlier and f_R to rise.

Why is retrotrapezoid nucleus no longer controlling f_R during REM sleep?

The transition from an autorhythmic homeostatically regulated state (anaesthesia, reduced preparations, non-REM sleep and quiet wake) to other forms of breathing (voluntary, emotional, REM sleep) is poorly understood. However, in general terms, the 'commanded' model, where inspiration is still triggered by the

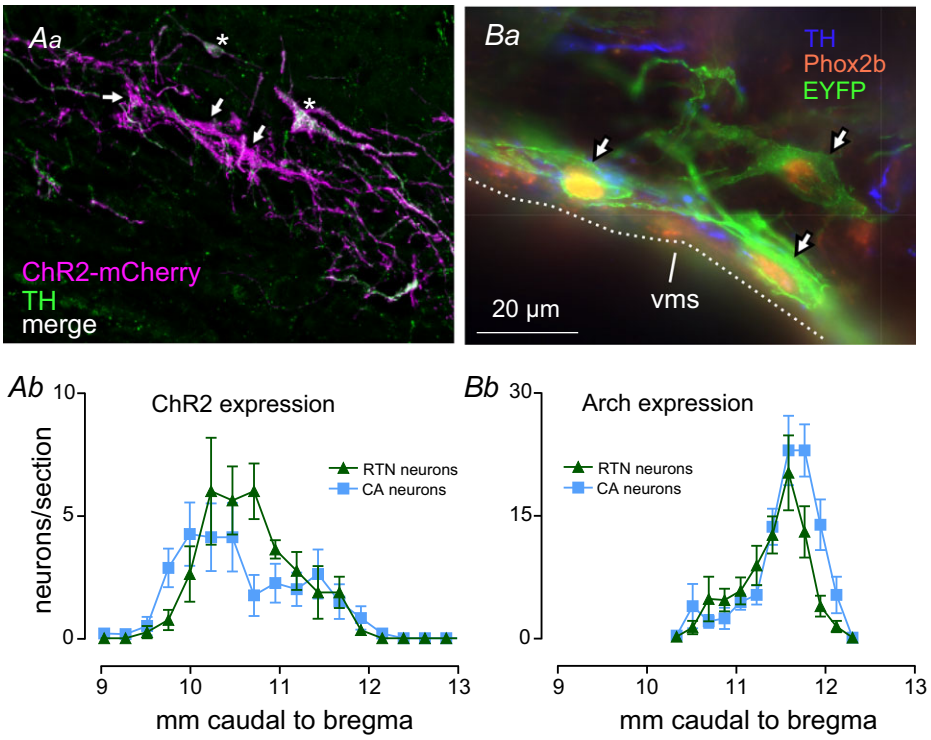

Figure 9. Location and phenotype of ChR2- or Arch-transduced neurons.
Aa, cluster of ChR2-transduced neurons within the rostral RTN (transverse plane; approximate location: 10.2 mm caudal to bregma). Three of five neurons were not TH-immunoreactive (arrows) and were presumptive RTN central respiratory chemoreceptors, the other two (stars) were TH-immunoreactive (A5 noradrenergic neurons). *Ab*, rostrocaudal distribution of ChR2-transduced RTN and catecholaminergic (CA) neurons (n = 8). Neurons were transduced on the left side of the brain only. *Ba*, three Arch-transduced putative RTN central respiratory chemoreceptor neurons (arrows) located next to the VMS (transverse section at ~11.4 mm caudal to Bregma; green: Arch-EYFP; blue: TH; red: Phox2b). *Bb*, rostrocaudal distribution of Arch-EYFP-transduced neurons (n = 8; RTN neurons = TH^-/$Phox2b^+$/EYFP; CA neurons: TH^+/ $Phox2b^+$/$EYFP^+$). Neurons were transduced bilaterally. Distance from bregma according to a standard rat atlas (Paxinos & Watson, 2005) (sections aligned using caudal end of facial motor nucleus as level 11.6 mm caudal to bregma). Calibration bar in *Ba* equals 100 μm (*Aa*) or 20 μm (*Ba*). CA, catecholamine; RTN, retrotrapezoid nucleus; TH, tyrosine hydroxylase; VMS, ventral medullary surface.

pontomedullary RPG, but its timing is tightly controlled by powerful inhibitory inputs from higher source(s) (Richter & Smith, 2014) seems the most plausible for several reasons. The pontomedullary RPG is clearly engaged during both REM sleep and volitional control (Lovering *et al.* 2006) and the integrity of the pre-Bötzinger circuitry is required for normal breathing during both REM and non-REM sleep (McKay & Feldman, 2008). Finally, given that RTN projections are propriobulbar (Bochorishvili *et al.* 2012), the homeostatic control of V_T during REM sleep must occur via the pontomedullary RPG.

Post-inspiratory inhibition is probably far more critical to the voluntary control of breathing than to breathing automaticity during quiet wake and non-REM sleep (Guz, 1997; Richter & Smith, 2014). The irregular breathing pattern present during REM sleep may share this characteristic. A plausible reason why RTN no longer controls f_R during REM sleep could be that the excitatory effect of RTN on the preI/I neurons is gated out during REM sleep by powerful inhibitory inputs from outside the pontomedullary RPG, which clamp the membrane potential of these neurons during the expiratory phase of the breathing cycle (Richter & Smith, 2014).

Physiological and pathophysiological relevance

The present observations could explain why many forms of central sleep apnoea, including CCHS occur predominantly during non-REM sleep (Berssenbrugge *et al.* 1983; Farney *et al.* 2003; Lovering *et al.* 2012). During REM sleep, V_E depends more on f_R, which rises while V_T decreases. Because f_R is no longer under chemoreceptor control during REM sleep, V_E is less dependent on P_{a,CO_2} than during non-REM sleep. Therefore, recurrent cycles of hyperventilation and apnoeas presumably cannot be sustained during REM sleep because, as shown here in rats, CRCs such as RTN contribute much less to ventilation.

Experimental limitations

PRSx8-based LVVs transduce a mixed population of RTN and catecholaminergic neurons as described before (Abbott *et al.* 2009; Marina *et al.* 2010; Abbott *et al.* 2011). In the ChR2 experiments, most transduced neurons (54%) were TH-negative hence putative CRCs. These neurons were located within the rostral half of RTN, which contains A5 noradrenergic neurons but few C1 adrenergic cells (Takakura *et al.* 2008). Selective C1 cell stimulation raises BP massively in conscious rats (Burke *et al.* 2014). Here BP was unaffected. Thus few C1 neurons could have been directly or synaptically activated and, consequently, these neurons could not have produced the observed breathing stimulation. Some contribution of A5 neuron stimulation to the breathing effects observed presently cannot be excluded.

For the loss of function experiments (Arch experiments), we needed to target the caudal RTN to transduce more CRCs. This region contains numerous C1 cells and, consequently, 56% of the Arch-transduced neurons were TH-immunoreactive. Under anaesthesia, Arch activation effectively silenced RTN neurons (Basting *et al.* 2015). In anaesthetized rats, sympathetic tone is

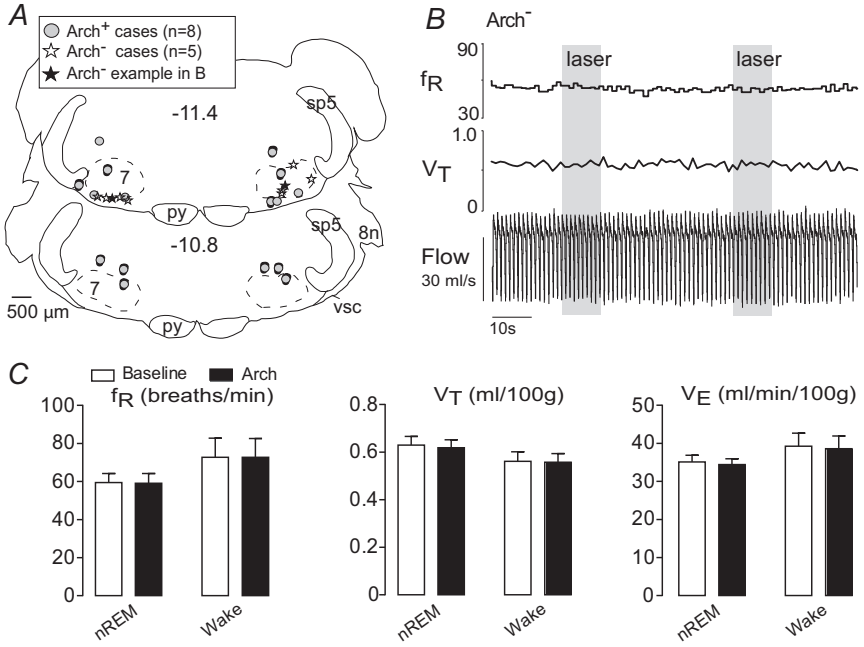

Figure 10. Photostimulation of the RTN in control animals has no effect on breathing.
A, location of the bilateral optic fibre tips identified in control rats (Arch$^-$; $n = 5$) and Arch-expressing rats (Arch$^+$; $n = 8$) overlap in the ventrolateral medulla. These sites are plotted on two transverse brain sections closest to their location. The tip sites of example B are represented by the filled star. Stereotaxic coordinates (transverse planes posterior to bregma) correspond to the atlas of Paxinos & Watson (2005). *B*, bilateral illumination of the RTN region with green light (10 s, ~5 mW) in an Arch$^-$ rat produced no change in breathing variables. *C*, group data from five Arch$^-$ animals show no effect of photostimulation of RTN with constant green light (10 s, ~5 mW) on breathing variables in either non-REM sleep or quiet wake states (two-way repeated measures ANOVA). nREM, non-REM; RTN, retrotrapezoid nucleus

high, the C1 cells are very active and their inhibition produces profound hypotension consistent with their sympathoexcitatory function (Schreihofer & Guyenet, 1997; Burke *et al.* 2008; Marina *et al.* 2011; Guyenet *et al.* 2013). Here, in conscious rats, Arch photostimulation had no effect on BP. One explanation is that sympathetic tone is low in resting unstressed and normoxic animals and the transduced C1 cells have a correspondingly low resting discharge. Another possibility is that the Arch-transduced C1 cells were inadequately hyperpolarized by the light. In any event, the lack of BP change indicates that C1 cell inhibition was minor at best. Consequently, a change in the activity of the C1 cells is very unlikely to have contributed significantly to the observed respiratory changes.

Summary and conclusions

RTN regulates both f_R and V_T when the pontomedullary RPG is autorhythmic (anaesthesia, non-REM sleep, quiet wake) but RTN no longer controls f_R during REM sleep. We speculate that during REM sleep, as during voluntary breathing, the expiratory phase of the breathing cycle is controlled by suprabulbar inputs that powerfully inhibit the pre-Bötzinger complex and shunt out the excitatory effect of RTN on the rhythmogenic core. A higher resting f_R that is no longer subject to control by RTN could explain the absence of periodic breathing and central sleep apnoea during REM sleep in humans.

References

Abbott SB, Stornetta RL, Fortuna MG, Depuy SD, West GH, Harris TE & Guyenet PG (2009). Photostimulation of retrotrapezoid nucleus phox2b-expressing neurons in vivo produces long-lasting activation of breathing in rats. *J Neurosci* **29**, 5806–5819.

Abbott SB, Stornetta RL, Coates MB & Guyenet PG (2011). Phox2b-expressing neurons of the parafacial region regulate breathing rate, inspiration, and expiration in conscious rats. *J Neurosci* **31**, 16410–16422.

Abbott SB, Coates MB, Stornetta RL & Guyenet PG (2013*a*). Optogenetic stimulation of C1 and retrotrapezoid nucleus neurons causes sleep state-dependent cardiorespiratory stimulation and arousal in rats. *Hypertension* **61**, 835–841.

Abbott SB, Depuy SD, Nguyen T, Coates MB, Stornetta RL & Guyenet PG (2013*b*). Selective optogenetic activation of rostral ventrolateral medullary catecholaminergic neurons produces cardiorespiratory stimulation in conscious mice. *J Neurosci* **33**, 3164–3177.

Abbott SB, Holloway BB, Viar KE & Guyenet PG (2014). Vesicular glutamate transporter 2 is required for the respiratory and parasympathetic activation produced by optogenetic stimulation of catecholaminergic neurons in the rostral ventrolateral medulla of mice in vivo. *Eur J Neurosci* **39**, 98–106.

Amiel J, Laudier B, Attie-Bitach T, Trang H, de PL, Gener B, Trochet D, Etchevers H, Ray P, Simonneau M, Vekemans M, Munnich A, Gaultier C & Lyonnet S (2003). Polyalanine expansion and frameshift mutations of the paired-like homeobox gene PHOX2B in congenital central hypoventilation syndrome. *Nat Genet* **33**, 459–461.

Ballantyne D & Richter DW (1986). The non-uniform character of expiratory synaptic activity in expiratory bulbospinal neurones of the cat. *J Physiol* **370**, 433–456.

Basting TM, Burke PG, Kanbar R, Viar KE, Stornetta DS, Stornetta RL & Guyenet PG (2015). Hypoxia silences retrotrapezoid nucleus respiratory chemoreceptors via alkalosis. *J Neurosci* **35**, 527–543.

Bautista TG, Burke PG, Sun QJ, Berkowitz RG & Pilowsky PM (2010). The generation of post-inspiratory activity in laryngeal motoneurons: a review. *Adv Exp Med Biol* **669**, 143–149.

Berssenbrugge A, Dempsey J, Iber C, Skatrud J & Wilson P (1983). Mechanisms of hypoxia-induced periodic breathing during sleep in humans. *J Physiol* **343**, 507–524.

Berthon-Jones M & Sullivan CE (1984). Ventilation and arousal responses to hypercapnia in normal sleeping humans. *J Appl Physiol* **57**, 59–67.

Bochorishvili G, Stornetta RL, Coates MB & Guyenet PG (2012). Pre-Botzinger complex receives glutamatergic innervation from galaninergic and other retrotrapezoid nucleus neurons. *J Comp Neurol* **520**, 1047–1061.

Brown DL & Guyenet PG (1985). Electrophysiological study of cardiovascular neurons in the rostral ventrolateral medulla in rats. *Circ Res* **56**, 359–369.

Burgess KR (1997). Central sleep apnoea and heart failure (Part I). *Respirology* **2**, 243–253.

Burke PG, Li Q, Costin ML, McMullan S, Pilowsky PM & Goodchild AK (2008). Somatostatin 2A receptor-expressing presympathetic neurons in the rostral ventrolateral medulla maintain blood pressure. *Hypertension* **52**, 1127–1133.

Burke PG, Abbott SB, Coates MB, Viar KE, Stornetta RL & Guyenet PG (2014). Optogenetic stimulation of adrenergic C1 neurons causes sleep state-dependent cardiorespiratory stimulation and arousal with sighs in rats. *Am J Respir Crit Care Med* **190**, 1301–1310.

Coote JH (1982). Respiratory and circulatory control during sleep. *J Exp Biol* **100**, 223–244.

Dejours P (1962). Chemoreflexes in breathing. *Physiol Rev* **42**, 335–358.

Dempsey JA, Smith CA, Blain GM, Xie A, Gong Y & Teodorescu M (2012). Role of central/peripheral chemoreceptors and their interdependence in the pathophysiology of sleep apnea. *Adv Exp Med Biol* **758**, 343–349.

Dobbins EG & Feldman JL (1994). Brainstem network controlling descending drive to phrenic motoneurons in rat. *J Comp Neurol* **347**, 64–86.

Doi A & Ramirez JM (2008). Neuromodulation and the orchestration of the respiratory rhythm. *Respir Physiol Neurobiol* **164**, 96–104.

Douglas NJ, White DP, Weil JV, Pickett CK, Martin RJ, Hudgel DW & Zwillich CW (1982*a*). Hypoxic ventilatory response decreases during sleep in normal men. *Am Rev Respir Dis* **125**, 286–289.

Douglas NJ, White DP, Weil JV, Pickett CK & Zwillich CW (1982*b*). Hypercapnic ventilatory response in sleeping adults. *Am Rev Respir Dis* **126**, 758–762.

Dutschmann M & Herbert H (2006). The Kolliker-Fuse nucleus gates the postinspiratory phase of the respiratory cycle to control inspiratory off-switch and upper airway resistance in rat. *Eur J Neurosci* **24**, 1071–1084.

Fagenholz SA, O'Connell K & Shannon DC (1976). Chemoreceptor function and sleep state in apnea. *Pediatrics* **58**, 31–36.

Farney RJ, Walker JM, Cloward TV & Rhondeau S (2003). Sleep-disordered breathing associated with long-term opioid therapy. *Chest* **123**, 632–639.

Feldman JL, Del Negro CA & Gray PA (2013). Understanding the rhythm of breathing: so near, yet so far. *Annu Rev Physiol* **75**, 423–452.

Fleming PJ, Cade D, Bryan MH & Bryan AC (1980). Congenital central hypoventilation and sleep state. *Pediatrics* **66**, 425–428.

Fraigne JJ & Orem JM (2011). Phasic motor activity of respiratory and non-respiratory muscles in REM sleep. *Sleep* **34**, 425–434.

Gestreau C, Heitzmann D, Thomas J, Dubreuil V, Bandulik S, Reichold M, Bendahhou S, Pierson P, Sterner C, Peyronnet-Roux J, Benfriha C, Tegtmeier I, Ehnes H, Georgieff M, Lesage F, Brunet JF, Goridis C, Warth R & Barhanin J (2010). Task2 potassium channels set central respiratory CO_2 and O_2 sensitivity. *Proc Natl Acad Sci USA* **107**, 2325–2330.

Gonzalez C, Almaraz L, Obeso A & Rigual R (1994). Carotid body chemoreceptors: from natural stimuli to sensory discharges. *Physiol Rev* **74**, 829–898.

Gourine AV, Kasymov V, Marina N, Tang F, Figueiredo MF, Lane S, Teschemacher AG, Spyer KM, Deisseroth K & Kasparov S (2010). Astrocytes control breathing through pH-dependent release of ATP. *Science* **329**, 571–575.

Gray PA, Rekling JC, Bocchiaro CM & Feldman JL (1999). Modulation of respiratory frequency by peptidergic input to rhythmogenic neurons in the PreBotzinger complex. *Science* **286**, 1566–1568.

Guyenet PG (2014). Regulation of breathing and autonomic outflows by chemoreceptors. *Compr Physiol* **4**, 1511–1562.

Guyenet PG & Mulkey DK (2010). Retrotrapezoid nucleus and parafacial respiratory group. *RespirPhysiol Neurobiol* **173**, 244–255.

Guyenet PG, Mulkey DK, Stornetta RL & Bayliss DA (2005). Regulation of ventral surface chemoreceptors by the central respiratory pattern generator. *J Neurosci* **25**, 8938–8947.

Guyenet PG, Stornetta RL & Bayliss DA (2010). Central respiratory chemoreception. *J Comp Neurol* **518**, 3883–3906.

Guyenet PG, Stornetta RL, Bochorishvili G, Depuy SD, Burke PG & Abbott SB (2013). C1 neurons: the body's EMTs. *Am J Physiol Regul Integr Comp Physiol* **305**, R187–R204.

Guz A (1997). Brain, breathing and breathlessness. *Respir Physiol* **109**, 197–204.

Han X, Chow BY, Zhou H, Klapoetke NC, Chuong A, Rajimehr R, Yang A, Baratta MV, Winkle J, Desimone R & Boyden ES (2011). A high-light sensitivity optical neural silencer: development and application to optogenetic control of non-human primate cortex. *Front Syst Neurosci* **5**, 18.

Haouzi P & Bell HJ (2009). Control of breathing and volitional respiratory rhythm in humans. *J Appl Physiol* **106**, 904–910.

Haxhiu MA, van Lunteren E, Mitra J & Cherniack NS (1987). Comparison of the response of diaphragm and upper airway dilating muscle activity in sleeping cats. *Respir Physiol* **70**, 183–193.

Horner RL (2009). Emerging principles and neural substrates underlying tonic sleep-state-dependent influences on respiratory motor activity. *Philos Trans R Soc Lond B Biol Sci* **364**, 2553–2564.

Horner RL, Liu X, Gill H, Nolan P, Liu H & Sood S (2002). Effects of sleep-wake state on the genioglossus *vs.* diaphragm muscle response to CO_2 in rats. *J Appl Physiol* **92**, 878–887.

Huckstepp RT & Dale N (2011). Redefining the components of central CO_2 chemosensitivity – towards a better understanding of mechanism. *J Physiol* **589**, 5561–5579.

Hwang DY, Carlezon WA, Jr, Isacson O & Kim KS (2001). A high-efficiency synthetic promoter that drives transgene expression selectively in noradrenergic neurons. *Hum Gene Ther* **12**, 1731–1740.

Janczewski WA & Feldman JL (2006). Distinct rhythm generators for inspiration and expiration in the juvenile rat. *J Physiol* **570**, 407–420.

Kanbar R, Stornetta RL, Cash DR, Lewis SJ & Guyenet PG (2010). Photostimulation of Phox2b medullary neurons activates cardiorespiratory function in conscious rats. *Am J Respir Crit Care Med* **182**, 1184–1194.

Lovering AT, Dunin-Barkowski WL, Vidruk EH & Orem JM (2003). Ventilatory response of the cat to hypoxia in sleep and wakefulness. *J Appl Physiol* **95**, 545–554.

Lovering AT, Fraigne JJ, Dunin-Barkowski WL, Vidruk EH & Orem JM (2006). Medullary respiratory neural activity during hypoxia in NREM and REM sleep in the cat. *J Neurophysiol* **95**, 803–810.

Lovering AT, Fraigne JJ, Dunin-Barkowski WL, Vidruk EH & Orem JM (2012). Tonic and phasic drive to medullary respiratory neurons during periodic breathing. *Respir Physiol Neurobiol* **181**, 286–301.

Marcus NJ, R. DR, Schultz EP, Xia XH & Schultz HD (2014). Carotid body denervation improves autonomic and cardiac function and attenuates disordered breathing in congestive heart failure. *J Physiol* **592**, 391–408.

Marina N, Abdala AP, Trapp S, Li A, Nattie EE, Hewinson J, Smith JC, Paton JF & Gourine AV (2010). Essential role of Phox2b-expressing ventrolateral brainstem neurons in the chemosensory control of inspiration and expiration. *J Neurosci* **30**, 12466–12473.

Marina N, Abdala AP, Korsak A, Simms AE, Allen AM, Paton JF & Gourine AV (2011). Control of sympathetic vasomotor tone by catecholaminergic C1 neurones of the rostral ventrolateral medulla oblongata. *Cardiovasc Res* **91**, 703–710.

Mattis J, Tye KM, Ferenczi EA, Ramakrishnan C, O'Shea DJ, Prakash R, Gunaydin LA, Hyun M, Fenno LE, Gradinaru V, Yizhar O & Deisseroth K (2012). Principles for applying optogenetic tools derived from direct comparative analysis of microbial opsins. *Nat Methods* **9**, 159–172.

McKay LC & Feldman JL (2008). Unilateral ablation of pre-Botzinger complex disrupts breathing during sleep but not wakefulness. *Am J Respir Crit Care Med* **178**, 89–95.

Mulkey DK, Stornetta RL, Weston MC, Simmons JR, Parker A, Bayliss DA & Guyenet PG (2004). Respiratory control by ventral surface chemoreceptor neurons in rats. *Nat Neurosci* **7**, 1360–1369.

Mulkey DK, Rosin DL, West G, Takakura AC, Moreira TS, Bayliss DA & Guyenet PG (2007). Serotonergic neurons activate chemosensitive retrotrapezoid nucleus neurons by a pH-independent mechanism. *J Neurosci* **27**, 14128–14138.

Nakamura A, Zhang W, Yanagisawa M, Fukuda Y & Kuwaki T (2007). Vigilance state-dependent attenuation of hypercapnic chemoreflex and exaggerated sleep apnea in orexin knockout mice. *J Appl Physiol* **102**, 241–248.

Ohashi S, Izumizaki M, Atsumi T & Homma I (2013). CO_2 homeostasis is maintained in conscious humans by regulation of tidal volume, but not of respiratory rhythm. *Respir Physiol Neurobiol* **186**, 155–163.

Orem JM, Lovering AT & Vidruk EH (2005). Excitation of medullary respiratory neurons in REM sleep. *Sleep* **28**, 801–807.

Pagliardini S, Janczewski WA, Tan W, Dickson CT, Deisseroth K & Feldman JL (2011). Active expiration induced by excitation of ventral medulla in adult anesthetized rats. *J Neurosci* **31**, 2895–2905.

Paxinos G & Watson C (2005). *The Rat Brain in Stereotaxic Coordinates*. Elsevier Academic Press, San Diego.

Potts JT, Rybak IA & Paton JF (2005). Respiratory rhythm entrainment by somatic afferent stimulation. *J Neurosci* **25**, 1965–1978.

Ramanantsoa N, Hirsch MR, Thoby-Brisson M, Dubreuil V, Bouvier J, Ruffault PL, Matrot B, Fortin G, Brunet JF, Gallego J & Goridis C (2011). Breathing without CO_2 chemosensitivity in conditional Phox2b mutants. *J Neurosci* **31**, 12880–12888.

Richter DW & Smith JC (2014). Respiratory rhythm generation in vivo. *Physiology (Bethesda)* **29**, 58–71.

Saper CB, Fuller PM, Pedersen NP, Lu J & Scammell TE (2010). Sleep state switching. *Neuron* **68**, 1023–1042.

Schreihofer AM & Guyenet PG (1997). Identification of C1 presympathetic neurons in rat rostral ventrolateral medulla by juxtacellular labeling in vivo. *J Comp Neurol* **387**, 524–536.

Smith CA, Henderson KS, Xi L, Chow C-M, Eastwood PR & Dempsey JA (1997). Neural-mechanical coupling of breathing in REM sleep. *J Appl Physiol* **83**, 1923–1932.

Smith JC, Abdala AP, Borgmann A, Rybak IA & Paton JF (2013). Brainstem respiratory networks: building blocks and microcircuits. *Trends Neurosci* **36**, 152–162.

Sparta DR, Stamatakis AM, Phillips JL, Hovelso N, van ZR & Stuber GD (2012). Construction of implantable optical fibers for long-term optogenetic manipulation of neural circuits. *Nat Protoc* **7**, 12–23.

Sullivan CE, Murphy E, Kozar LF & Phillipson EA (1979). Ventilatory responses to CO_2 and lung inflation in tonic versus phasic REM sleep. *J Appl Physiol* **47**, 1305–1310.

Sun QJ, Berkowitz RG & Pilowsky PM (2008). GABA A mediated inhibition and post-inspiratory pattern of laryngeal constrictor motoneurons in rat. *Respir Physiol Neurobiol* **162**, 41–47.

Takakura AC, Moreira TS, Stornetta RL, West GH, Gwilt JM & Guyenet PG (2008). Selective lesion of retrotrapezoid Phox2b-expressing neurons raises the apnoeic threshold in rats. *J Physiol* **586**, 2975–2991.

Tupal S, Huang WH, Picardo MC, Ling GY, Del Negro CA, Zoghbi HY & Gray PA (2014). Atoh1-dependent rhombic lip neurons are required for temporal delay between independent respiratory oscillators in embryonic mice. *Elife* **3**, e02265.

Veasey SC, Fornal CA, Metzler CW & Jacobs BL (1995). Response of serotonergic caudal raphe neurons in relation to specific motor activities in freely moving cats. *J Neurosci* **15**, 5346–5359.

Wang S, Benamer N, Zanella S, Kumar NN, Shi Y, Bevengut M, Penton D, Guyenet PG, Lesage F, Gestreau C, Barhanin J & Bayliss DA (2013). TASK-2 channels contribute to pH sensitivity of retrotrapezoid nucleus chemoreceptor neurons. *J Neurosci* **33**, 16033–16044.

Weese-Mayer DE, Berry-Kravis EM, Ceccherini I, Keens TG, Loghmanee DA & Trang H (2010). An official ATS clinical policy statement: Congenital central hypoventilation syndrome: genetic basis, diagnosis, and management. *Am J Respir Crit Care Med* **181**, 626–644.

Weil JV (2004). Sleep at high altitude. *High Alt Med Biol* **5**, 180–189.

Yokota S, Oka T, Tsumori T, Nakamura S & Yasui Y (2007). Glutamatergic neurons in the Kolliker-Fuse nucleus project to the rostral ventral respiratory group and phrenic nucleus: a combined retrograde tracing and in situ hybridization study in the rat. *Neurosci Res* **59**, 341–346.

Additional information

Competing interests

None.

Author contributions

P.G.R.B., R.L.S., T.M.B. and P.G.G. designed the experiments. P.G.R.B., R.K. and T.M.B. performed and analysed the physiological experiments. W.M.H., K.E.V. and R.L.S. did the histology. P.G.R.B. and P.G.G. wrote the manuscript.

Funding

This work was supported by National Institutes of Health Grants HL28785 and HL74011 to P.G.G.

Supporting information

The following supporting information is available in the online version of this article.

Videos S1
Videos S2
Videos S3
Videos S4